

Article

Effect of Heat Treatment on the Corrosion Resistance of AlFeCoNiMo_{0.2} High-Entropy Alloy in NaCl and H₂SO₄ Solutions

Yuhan Peng^{1,2}, Ge Zhou^{1,2,*}, Jinke Han^{1,2}, Jianlin Li^{1,2}, Haoyu Zhang^{1,2} , Siqian Zhang^{1,2}, Li Lin^{1,2}, Lijia Chen^{1,2} and Xue Cao³

¹ School of Materials Science and Engineering, Shenyang University of Technology, Shenyang 110870, China

² Shenyang Key Laboratory of Advanced Structural Materials and Applications, Shenyang University of Technology, Shenyang 110870, China

³ Beijing Institute of Aeronautical Materials of China Aviation Development, Beijing 100094, China

* Correspondence: zhouge@sut.edu.cn

Abstract: The effects of casting and different heat treatment processes on the corrosion resistance of AlFeCoNiMo_{0.2} high-entropy alloy in 3.5% NaCl (mass fraction) and 0.5 mol/L H₂SO₄ solutions were investigated using dynamic potential polarization curves, SEM, XRD, XPS, and other test methods. The results show that in the Cl⁻ environment, the cast alloy has the lowest corrosion current density and higher corrosion resistance compared to the annealed alloy. The elements Al and Mo are severely segregated in the crystal and in the grain boundaries, where galvanic corrosion occurs, and the Al-rich phase produces pitting corrosion in the crystal. The main components of its passive film are oxides of Al, Fe, Co, and Mo, and oxides and hydroxides of Ni. In the SO₄²⁻ environment, the best corrosion resistance is achieved in the 900 °C annealed state of the alloy. Electrochemical test results show that the alloys all undergo secondary passivation, producing two successive product films to protect the metal matrix. Preferential corrosion areas are concentrated in the molybdenum-rich grain boundaries and nearby dendritic regions, reducing the corrosion resistance of the alloy. The main components of the passive film are oxides of Al and Mo; oxides of Fe, Co, Ni; and hydroxides. The Mo element in the passive film prevents the activated dissolution of Fe and produces the protective component MoO₃, which inhibits the dissolution of the alloy and improves the stability of the passive film. The presence of Mo elements increases the selective dissolution of Fe, and the aggregation of Mo elements at grain boundaries after annealing weakens the corrosion resistance of the alloy and leads to the dissolution of the passive film. The main components of the passive film are oxides of Al and Mo; oxides of Fe, Co, Ni; and hydroxides.

Keywords: AlFeCoNiMo_{0.2} high-entropy alloy; heat treatment; corrosion resistance; microstructure



Citation: Peng, Y.; Zhou, G.; Han, J.; Li, J.; Zhang, H.; Zhang, S.; Lin, L.; Chen, L.; Cao, X. Effect of Heat Treatment on the Corrosion Resistance of AlFeCoNiMo_{0.2} High-Entropy Alloy in NaCl and H₂SO₄ Solutions. *Metals* **2023**, *13*, 849. <https://doi.org/10.3390/met13050849>

Academic Editors: Sundeeep Mukherjee and Jiro Kitagawa

Received: 12 March 2023

Revised: 18 April 2023

Accepted: 20 April 2023

Published: 26 April 2023



Copyright: © 2023 by the authors. Licensee MDPI, Basel, Switzerland. This article is an open access article distributed under the terms and conditions of the Creative Commons Attribution (CC BY) license (<https://creativecommons.org/licenses/by/4.0/>).

1. Introduction

High-entropy alloys (HEAs) are novel alloys composed of four or more metallic elements with an atomic fraction between 5% and 35% for each alloying element. All high-entropy alloys exist in solid solution form, usually in the form of single-phase FCC or single-phase BCC structures or mixed FCC and BCC phase compositions, and despite the inclusion of more significant elements, no complicated intermetallic compounds or brittle phases are formed between the elements [1–4]. High-entropy alloys have unique properties, such as high fracture toughness [5,6], high creep resistance [7,8], high oxidation and corrosion resistance [9,10], etc., due to the serious lattice distortion and slow diffusion effect that the solid-solution phase in HEAs possesses under this design concept. Corrosion resistance is a topic that is addressed in a variety of special service environment areas, including aerospace, nuclear engineering, marine engineering, and others.

Since high-entropy alloys have a strong potential for use in corrosion resistance, academics and organizations conducting related research both domestically and internationally have conducted extensive research on the corrosion behavior of alloying elements in various HEA systems under various corrosive environments and heat-treatment process conditions. As a result, many significant research findings have been made. Chou et al. [11] investigated the influence of Mo element content on the corrosion behavior of $\text{Co}_{1.5}\text{CrFeNi}_{1.5}\text{Ti}_{0.5}\text{Mo}_x$ HEAs in various solution environments and different heat-treatment states and confirmed that, in a NaCl solution environment, the corrosion resistance of the alloy is improved with increases in Mo element content, and pitting corrosion is not readily induced. An $\text{Al}_x\text{CoCrFeNi}$ high-entropy alloy in H_2SO_4 solution underwent electrochemical corrosion, and Wang, Chou, and Kao et al. [12–14] examined the impact of Al content on this behavior. They also identified the features of the passivation film generation throughout the corrosion process. According to the findings, the Al content of the SO_4^{2-} medium is critical for the formation of the passive film. As the Al percentage varies, the resultant passive film takes on a porous appearance and impacts the ability of the alloy to resist corrosion. Based on this, Kao et al. [14] introduced Cl^- to H_2SO_4 solutions and discovered that the influence of Al elements on the pitting behavior of the alloy increased in SO_4^{2-} and Cl^- solutions, with more severe pitting occurring as the quantity of Al elements rose. In their investigation of the corrosion behavior of single-phase CoCrFeNi HEA in NaCl solution, Yang et al. [15] discovered that Cr, Ni, and other readily passivated metal components may significantly increase the corrosion resistance of the high-entropy alloy. The aforementioned study findings demonstrate that alloying element addition and content management have a significant impact on the corrosion behavior of high-entropy alloys, providing a theoretical foundation for the development of high-entropy alloys with superior corrosion performance.

Researchers started focusing on the impact of microstructures on the corrosion resistance of alloys under various heat-treatment states as the development of high-entropy alloys progressed, based on the challenge of alloy-composition design. Niu et al. [16,17] investigated the corrosion resistance of a high-entropy alloy in the $(\text{CoCrFeNi})_{100-x}\text{Mo}_x$ ($x = 1, 2, 3$) system under various heat-treatment regimes. The findings revealed that the corrosion resistance of the alloy increased with higher annealing temperatures and holding times, and the aforementioned phenomenon was especially notable when Mo element content was high. According to Lin et al. [18], the $\text{Cu}_{0.5}\text{CoCrFeNi}$ high-entropy alloy underwent a high-temperature aging treatment that successfully reduced the segregation of Cu components and resulted in a significant enhancement in the capacity to resist corrosion in the presence of NaCl solution. According to Wen et al. [19], the NiCrCoTiV HEA suffered a back-solution effect on the precipitated phases during heat treatment, resulting in a reduction in the quantity of precipitated phases and an increase in the corrosion resistance of the alloy. The effect of heat treatment on the corrosion resistance of AlFeNiCoCuCr in 3.5 wt% NaCl solution was investigated by Zhang et al. [20]. The results revealed that the alloy showed significant dendrite growth and a more compact microstructure after annealing at 1000 °C, which improved the corrosion resistance of the alloy. In terms of the homogeneity of alloy components, phase precipitation, transformation, etc., this suggests that the heat-treatment procedure may manage the microstructure of high-entropy alloys. The information above suggests that alloy microstructure modification will be crucial to its ability to resist corrosion. Therefore, it is crucial to do research on the corrosion behavior of high-entropy alloys as well as various heat-treatment techniques.

In this paper, for the single-phase BCC structure $\text{AlFeCoNiMo}_{0.2}$ high-entropy alloy developed and designed independently, three temperatures of 800 °C, 900 °C, and 1000 °C were selected to carry out heat-treatment process tests, and electrochemical test methods were used to study the electrochemical corrosion behavior of the alloy in NaCl and H_2SO_4 media. Through electrochemical test analysis and passive film composition analysis, combined with SEM, XPS, and other test characterization results, the corrosion behavior and mechanism of the alloy under different heat-treatment conditions were revealed, thus providing theoretical support for the practical application of the alloy.

2. Materials and Methods

The experimental material was a self-designed AlFeCoNiMo_{0.2} high-entropy alloy. Preparation was based on the molar ratio of 1:1:1:1:0.2. Cylindrical ingots were obtained through repeated melting four times in a vacuum self-consumption furnace under Ar gas protection, and the alloy was ensured to be consistent with the nominal composition content via an inductively coupled plasma spectroscopy (ICP) generator, and the composition is shown in Table 1.

Table 1. Chemical composition (wt%) of the AlFeCoNiMo_{0.2} high-entropy alloy.

Al	Fe	Co	Ni	Mo
12.28	25.40	26.86	26.721	8.78

Figure 1a shows the IPF inverse polar diagram of the as-cast AlFeCoNiMo_{0.2} high-entropy alloy. The BCC solid-solution structure did not undergo phase transformation. The ingots were cut into small 10 mm × 10 mm × 5 mm squares using wire cutting, and some of the specimens were used for as-cast analysis. The alloy in the vacuum quartz tube was annealed at 800 °C, 900 °C, and 1000 °C and held for 1 h. The annealed alloy was then cooled in water. After being polished with 240, 600, and 1500 grit sandpaper in turn, the heat-treated samples were polished to a mirror-like finish on a metallographic polishing machine (WX100), and then they were ultrasonically cleaned. The crystalline structure of HEAs was identified using X-ray diffraction (XRD, Shimadzu XRD-7000, Kyoto, Japan) and a scanning range of 20°~90° with a scanning rate set to 4°/step.

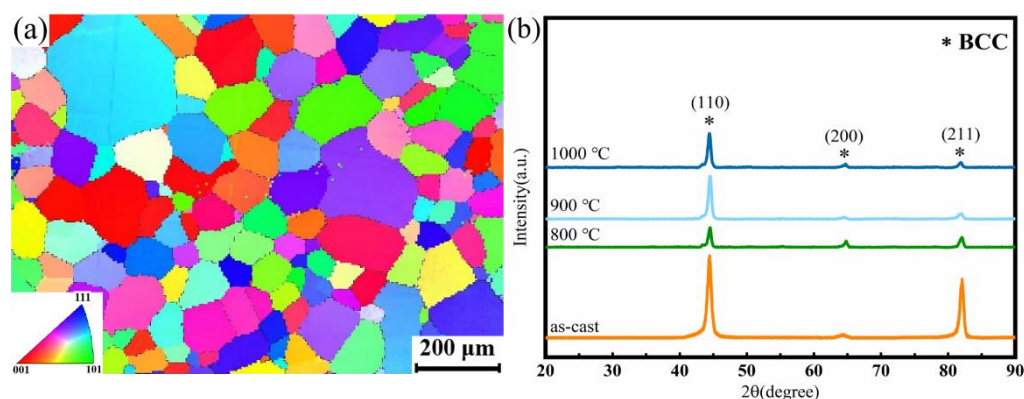


Figure 1. (a) IPF antipode diagram of the as-cast AlFeCoNiMo_{0.2} HEA and (b) XRD patterns of the as-cast and heat-treated AlFeCoNiMo_{0.2} HEA.

A VSP-300 electrochemical workstation was used to conduct the electrochemical experiments. The samples were employed as the working electrode, platinum wire served as the auxiliary electrode, and a saturated calomel electrode (SCE) served as the reference electrode in a three-electrode system. For 5000 s, the open-circuit potential (OCP) was observed. Electrochemical impedance spectroscopy (EIS) was carried out at 100 kHz~10 MHz with an amplitude of 10 mV after waiting for the state to stabilize. The dynamic potential polarization experiment used a 0.5 mV/s scan rate with a -1.5 V (vs. E_{OCP}) to 2.5 V (vs. E_{OCP}) scan potential range. Constant potential polarization was carried out at 0.5 V_{SCE} and 1 V_{SCE} in a solution environment of 3.5 wt% NaCl and 0.5 M H₂SO₄ for 3 h to form a stable passive film. To confirm the correctness of the data, every electrochemical test was carried out at room temperature at least twice under the exact same conditions. After the electrochemical tests, the surface composition of the passivated film was analyzed by scanning electron microscopy (SEM, Zeiss Gemini SEM 300) and X-ray photoelectron spectroscopy (XPS, Shimadzu Ax-is Uitra DLD, Japan).

3. Experiments and Results

3.1. AlFeCoNiMo_{0.2} High-Entropy Alloy Corrosion Morphology and Electrochemical Behavior in 3.5 wt% NaCl Solution

Figure 2 displays the polarization curves for cast and heat-treated AlFeCoNiMo_{0.2} HEAs with corrosion potential (E_{corr}) and corrosion current density (I_{corr}) shown in Table 2. After 5000 s, when the potential was largely steady, measurements of the polarization curve began. Figure 2 shows that the polarization curve at a higher voltage range lacks any evident passivation. This indicates that the corrosion products produced by the reaction have strong electrical conductivity and that, at high voltages, the corrosion currents of various heat-treated alloys do not increase and even show a tendency to decrease. Table 2 shows that there is no significant difference between the change in corrosion potential before and after heat treatment, which implies that there is no difference in the tendency to corrode in 3.5 wt% NaCl solution before and after heat treatment. However, the corrosion current density I_{corr} of the alloy after heat treatment is greater than that of the cast state, indicating that the cast state possesses better corrosion resistance. When different annealing temperatures are compared, one can see that the corrosion current density is lowest at 900–1 h, suggesting that the corrosion rate of the AlFeCoNiMo_{0.2} HEA is lower at 900–1 h than it is at 800–1 h and 1000–1 h. One of the factors influencing the change in corrosion current density is the simultaneous occurrence of dendritic development and modifications to grain boundary states at various annealing temperatures. Due to the presence of a large amount of Fe and Ni elements in the AlFeCoNiMo_{0.2} high-entropy alloy with a higher molar percentage than Mo elements, a potential difference due to the uneven distribution of the elements occurs, which reduces the stability of the passive film and is one of the reasons why the passive film is struck by current and produces a secondary passivation phenomenon.

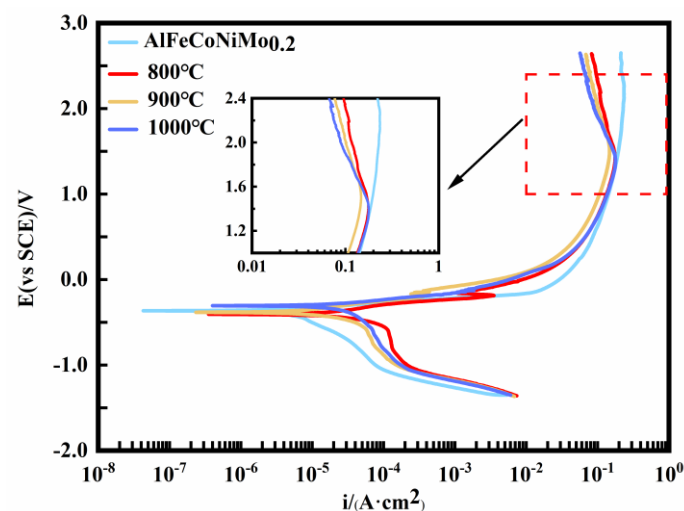


Figure 2. Potentiodynamic polarization curves of the AlFeCoNiMo_{0.2} HEA under as-cast conditions and after different heat treatments in 3.5 wt% NaCl solution.

Table 2. Electrochemical parameters of the AlFeCoNiMo_{0.2} high-entropy alloy under as-cast conditions and after different heat treatments in 3.5 wt% NaCl solution.

Material	Temperature (°C)	E_{corr} (mV)	I_{corr} ($\mu\text{A}\cdot\text{cm}^{-2}$)
AlFeCoNiMo _{0.2}	as-cast	−337.83 (± 4.88)	3.90 (± 0.31)
	800 °C	−347.87 (± 4.21)	31.07 (± 0.48)
	900 °C	−325.91 (± 4.24)	13.92 (± 0.44)
	1000 °C	−310.15 (± 3.92)	22.48 (± 0.39)

Figure 3 shows the surface morphology of the AlFeCoNiMo_{0.2} high-entropy alloy after polarization in 3.5 wt% NaCl solution. It is obvious that due to the difference in annealing temperatures, there is a large difference between the corrosion profiles of the

specimens and that the surface of the alloy is corroded to a more serious degree after annealing. As can be seen from Figure 3a, the as-cast alloy shows a dendritic structure with inconspicuous grain boundaries and deep corrosion pits on the surface, but the number is relatively small; the corrosion pits on the surface of the alloy increased significantly after heat treatment, but the corrosion did not occur at the grain boundaries, which shows that the corrosion resistance of the grain boundaries is stronger than that of the grain. The alloy showed more severe corrosion after the heat treatment of 800-1 h, which corresponds to the highest corrosion current density in Table 2 and the appearance of a significant number of corrosion pits that had a propensity to grow along the grain boundaries (Figure 3b). The corrosion pits were more numerous when the heat treatment was 1000-1 h, but the depth was shallow and did not occur along the grain boundary expansion (Figure 3d). When the alloy was heat-treated at 900-1 h, relatively straight grain boundaries appeared, and the intercrystalline organization was dendritic with the lowest number of etch pits compared to the other heat-treatment states (Figure 3c). There is an inextricable relationship between alloy corrosion morphology and chloride, and differences in morphology may indicate that different alloys in different annealed states may lead to differences in the mechanism of pit formation. This is consistent with the results of the polarization curves after polarization in 3.5 wt% NaCl solution. To further analyze the effect of heat treatment on the corrosion resistance and elemental distribution of the AlFeCoNiMo_{0.2} high-entropy alloy, samples from the as-cast and 900-1 h states were selected for EDS surface scanning, as shown in Figure 4. The Mo elements are found to be biased at the grain boundaries in the as-cast state. During heat treatment, the dendrites surrounding the grain boundaries grow and become more enriched with Mo elements, whereas the Al elements start to significantly accumulate within the grains, and there is an Al depletion at the grain boundaries. During heat treatment, the bias of the elements becomes more pronounced, indicating an increase in the likelihood of galvanic corrosion, with Al elements being more active than Mo elements and an increase in corrosion in Al-rich areas, which may also be a cause of intragrain corrosion. At the same time, when the passivated film area is attacked at one location, the Cl⁻ ions in the vicinity of the hole adsorb into the hole, which leads to an increase in the corrosion rate inside the hole, while the surface location on the outside of the hole has less tendency to corrode, which makes the hole size larger due to the difference in corrosion rate between the two location points [21].

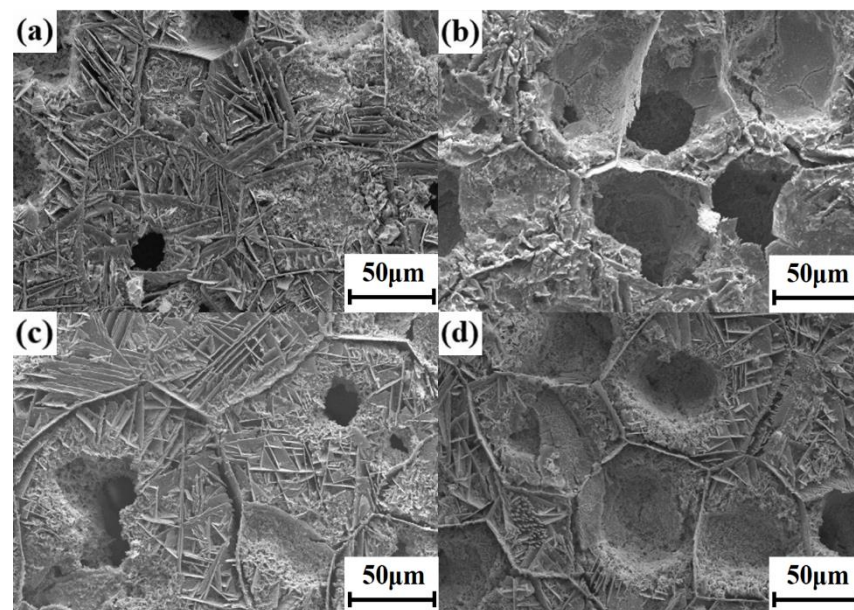


Figure 3. SEM images of the as-cast and different heat-treated AlFeCoNiMo_{0.2} HEAs after polarization in 3.5 wt% NaCl solution: (a) as-cast, (b) 800-1 h, (c) 900-1 h, and (d) 1000-1 h.

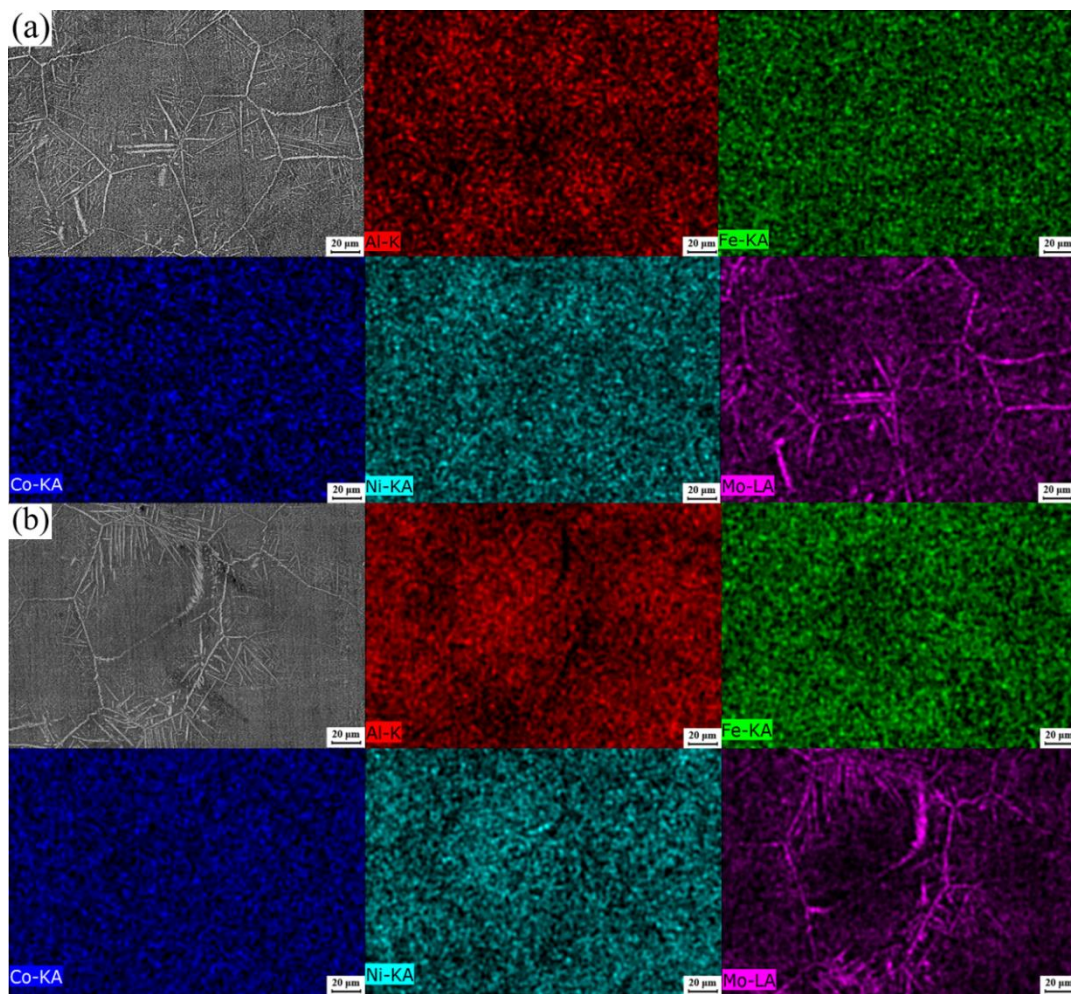


Figure 4. EDS mapping images of the surface of high-entropy alloys samples: (a) as-cast and (b) 900-1 h.

3.2. $\text{AlFeCoNiMo}_{0.2}$ High-Entropy Alloy Corrosion Morphology and Electrochemical Behavior in 0.5 M H_2SO_4 Solution

The potential polarization curves of the cast and various heat-treated $\text{AlFeCoNiMo}_{0.2}$ HEAs are shown in Figure 5 in a solution of 0.5 M H_2SO_4 . According to Figure 5, it is clear that passivation and over-passivation occurred in the polarization curves of $\text{AlFeCoNiMo}_{0.2}$ high-entropy alloys both as-cast and after heat treatment. This shows that a passive film was created on the alloy surface during anodic polarization, somewhat lessening the attack of aggressive anions. We observe that the polarization curve only exists in the region of the activation–passivation transition; since secondary passivation is a non-stable state and there is no stable passivation zone, it occurs throughout the corrosion process. The first passivation of the alloy produces corrosion products that stick to the surface of the substrate and obstruct subsequent reactions. The defenses of the substrate were weakened as the voltage increased, exposing the substrate to the solution directly, which increased current. The integrity of the passive film was also damaged. Because the working voltage increased and the passive film developed a second, larger passive region on the alloy surface, the polarization curve in Figure 5 fluctuated. The corrosion potential (E_{corr}) and corrosion current density (I_{corr}) determined by the polarization curve are displayed in Table 3. It is clear that the cast condition and 900-1 h have the lowest corrosion current density and the greatest corrosion resistance. Because sulfuric acid is an oxidizing acid, a significant quantity of H^+ serves as the primary corrosive medium. On the surface of the specimen, the passive film began to dissolve due to overpassivation. It is common to think of the passivation layer that the metal forms in the medium as an oxide or hydroxide that enables the anodic dissolution rate of the metal to be kept at a low level. $\text{AlFeCoNiMo}_{0.2}$ HEA is

the alloy discussed in the study. One of the causes of the current breakdown of the passive film and the secondary passivation phenomenon is the presence of significant amounts of Fe and Ni elements, which have higher molar percentages than Mo elements in the elemental distribution. This leads to potential differences, which in turn reduce the stability of the passive film. The aforementioned results are consistent with what has been written published in the literature [22].

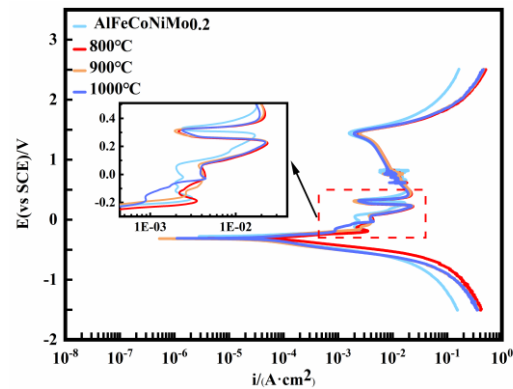


Figure 5. Potentiodynamic polarization curves of the AlFeCoNiMo_{0.2} HEA under as-cast conditions and after different heat treatments in 0.5 M H₂SO₄ solution.

Table 3. Electrochemical parameters of the AlFeCoNiMo_{0.2} high-entropy alloy under as-cast conditions and after different heat treatments in 0.5 M H₂SO₄ solution.

Material	Temperature (°C)	E _{corr} (mV)	I _{corr} (μA·cm ⁻²)
AlFeCoNiMo _{0.2}	as-cast	-275.33 (±3.81)	20.58 (±0.81)
	800 °C	-304.64 (±4.02)	51.73 (±1.01)
	900 °C	-305.08 (±3.96)	17.04 (±0.76)
	1000 °C	-293.88 (±4.18)	27.23 (±0.98)

Figure 6 shows the surface morphology of the AlFeCoNiMo_{0.2} high-entropy alloy after polarization in 0.5 M H₂SO₄ solution. As shown in Figure 6, following polarization, distinct levels of corrosion developed on the surfaces of cast and heat-treated AlFeCoNiMo_{0.2} HEAs. After corrosion of the alloy as cast (Figure 6a), it can be seen that the grain boundaries and the dendrites gathered near the grain boundaries have corroded, and there are also many shallow corrosion pits in the grains. The Mo elements of the alloy are more evenly distributed in the as-cast state, with some Mo elements in the grain boundaries and dendrites biased. After the alloy underwent 800-1 h heat treatment, Mo elements began to form dendrites in the crystal and gradually moved to the grain boundary in the form of dendrites, resulting in a larger corrosion crater on the surface of the alloy, an expansion along the grain boundary to produce a certain depression, and the intracrystalline dendrites also exhibited more serious corrosion (Figure 6b). After heat treatment of the alloy at 900-1 h, by this time, the Mo elements in the alloy had gathered and pinned at the grain boundaries and were evenly distributed, producing only light corrosion surfaces at the grain boundaries and nearby dendrites with no obvious pits (Figure 6c). When the alloy was heat-treated for 1000-1 h, the Mo element began to accumulate excessively in the grain boundaries and dendrites, and significant coarsening occurred at the grain boundaries as well as at the dendrites (Figure 6d). The above results are consistent with the trend of the self-corrosion current density of the alloy. The main reason for these results is that after heat treatment, the AlFeCoNiMo_{0.2} high-entropy alloy is enriched with Mo elements at the grain boundaries, and Mo elements have poor corrosion resistance in sulfuric acid solutions, leading to a decrease in the corrosion resistance of Mo-rich tissue structures in the metal grains in H₂SO₄ solutions and exacerbating the degree of corrosion dissolution in this region of the tissue structure.

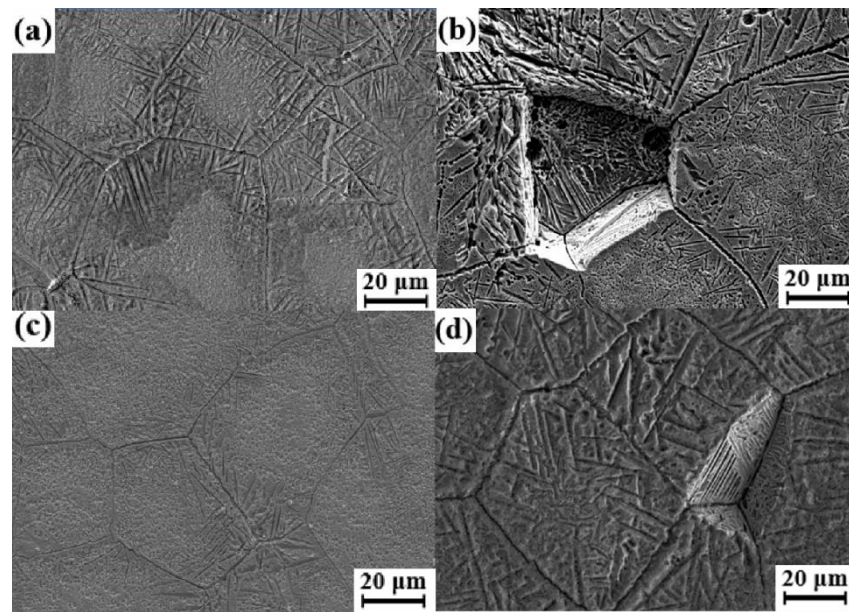


Figure 6. SEM images of the as-cast and different heat-treated AlFeCoNiMo_{0.2} high-entropy alloy after polarization in 0.5 M H₂SO₄ solution: (a) as-cast, (b) 800-1 h, (c) 900-1 h, and (d) 1000-1 h.

4. Analysis and Discussion

4.1. Electrochemical Impedance Spectroscopy (EIS) Analysis

Due to the high impedance of the passive film during the electrochemical reaction, which may effectively minimize corrosion current density (I_{corr}), the corrosion products produced by the passive film or surface are protective of the alloy substrate. The test technique using EIS enables the determination of the impedance magnitude of corrosion products produced by passive films or surfaces and reveals the corrosion process of the AlFeCoNiMo_{0.2} high-entropy alloy. Figure 7a,b show the Nyquist plots of the AlFeCoNiMo_{0.2} HEA in the as-cast condition and following various heat treatments in two solution media. Both the as-cast and heat-treated alloys exhibit semicircular properties, as shown in Figure 7a, which are connected to the charge transfer process taking place at the interface [23]. The cast alloy has the biggest arc radius of the group, suggesting that it has the highest corrosion resistance and the strongest resistance to charge transfer. Additionally, when the alloy underwent heat treatment, the arc radius shrank and peaked at 800-1 h, which was in line with the findings of the dynamic potential polarization curve in 3.5 wt% NaCl solution. The radius of the arc in 0.5 M H₂SO₄ solution reaches its maximum at 900-1 h and is closest to the as-cast condition when the corrosion resistance of the alloy is greater and the corrosion current density is lowest, as can be shown in Figure 7b. The alloy also exhibits poor corrosion resistance and the maximum corrosion current density at 800-1 h, when the arc radius is the lowest, which is similar to the changing pattern of the corrosion current density of the AlFeCoNiMo_{0.2} high-entropy alloy shown in Table 3.

The equivalent circuit diagram of the as-cast and annealed high-entropy alloy in these two different media are shown in Figure 7c, and the electrochemical impedance parameters of these two different media are summarized in Tables 4 and 5, respectively, to provide insight into the mechanism underlying the corrosion behavior. The solution resistance is represented by R_s , and the film resistance, by R_f . R_{ct} stands for charge transfer resistance, which is the impedance created by the kinetic control of an electrochemical process. The constant phase elements CPE1 and CPE2 are bilayer capacitors and passivated film capacitors, respectively. Table 4 demonstrates that the R_{ct} at 1000-1 h in NaCl solution is the lowest and that the other three states of the alloy do not significantly differ from one another. Comparing R_f , as-cast > 900-1 h > 1000-1 h > 800-1 h. It is clear that heat treatment in the Cl⁻ environment somewhat weakens the corrosion resistance of the AlFeCoNiMo_{0.2} high-entropy alloy. As-cast, 900-1 h, and 1000-1 h samples have n_1 and n_2 values that are

neener to 1. Thus, the system is closer to the ideal capacitance system. It can be seen that heat treatment in a Cl^- environment reduces the corrosion resistance of the $\text{AlFeCoNiMo}_{0.2}$ high-entropy alloy to some extent.

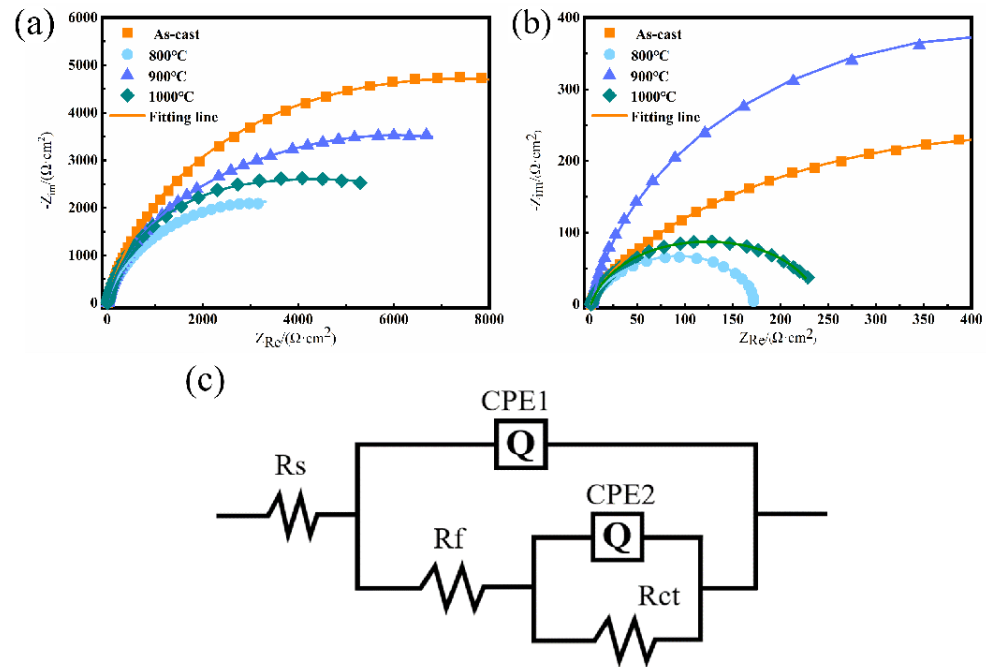


Figure 7. Nyquist plots of cast and heat-treated $\text{AlFeCoNiMo}_{0.2}$ HEA in (a) 3.5 wt% NaCl solution and (b) 0.5 M H_2SO_4 solution and (c) equivalent circuit for fitting the EIS experimental data.

Table 4. Equivalent circuit parameters for EIS of $\text{AlFeCoNiMo}_{0.2}$ HEA under as-cast conditions and different heat treatments in 3.5 wt% NaCl solution.

Condition	Solution	R_s (ohm)	R_f (ohm)	R_{ct} (ohm)	CPE1		CPE2	
					Y1 (F)	n1	Y2 (F)	n2
As-cast	3.5 wt% NaCl	8.098	9656	5448	1.039×10^{-4}	0.8583	5.469×10^{-4}	0.7459
800-1 h		7.751	1944	5762	7.516×10^{-5}	0.8778	1.558×10^{-4}	0.4889
900-1 h		10.05	5630	6143	8.886×10^{-5}	0.8614	2.941×10^{-4}	0.6862
1000-1 h		8.041	5438	3527	8.641×10^{-5}	0.8769	6.602×10^{-4}	0.7862

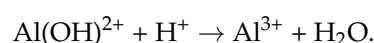
Table 5 shows that for both R_{ct} and R_f , the resistance values for 900-1 h and cast samples are greater in 0.5 M H_2SO_4 solution. The fitted values are more compatible with the actual observed values at 900-1 h because the n1 and n2 values are close to 1. It can be seen that the selection of a suitable temperature for annealing the $\text{AlFeCoNiMo}_{0.2}$ alloy in a sulfuric acid environment is effective in improving the corrosion resistance of the alloy.

Table 5. Equivalent circuit parameters for EIS of $\text{AlFeCoNiMo}_{0.2}$ HEA under as-cast conditions and different heat treatments in 0.5 M H_2SO_4 solution.

Condition	Solution	R_s (ohm)	R_f (ohm)	R_{ct} (ohm)	CPE1		CPE2	
					Y1 (F)	n1	Y2 (F)	n2
As-cast	0.5 mol/L H_2SO_4	1.841	353.7	1063	1.051×10^{-4}	0.9341	8.139×10^{-4}	0.8713
800-1 h		1.857	117	55.63	3.804×10^{-4}	0.8675	6.648×10^{-4}	0.9155
900-1 h		2.705	866.1	22.85	2.62×10^{-4}	0.9074	2.807×10^{-2}	0.9787
1000-1 h		3.193	208.6	31.18	2.938×10^{-4}	0.8456	2.538×10^{-4}	0.9586

4.2. XPS Analysis of Alloy Passive Films

In order to investigate in depth the passivation mechanism of the AlFeCoNiMo_{0.2} high-entropy alloy in the two different ionic environments above, the chemical composition and elemental valence states of the passive film on the surface of the alloy after polarization were analyzed using XPS, and the results are shown in Figures 8 and 9. The spectra of Al 2p, Fe 2p, Co 2p, Ni 2p, and Mo 3d in 3.5 wt% NaCl solution are shown in Figure 8. It is clear from the figure that the passive films of this metal all contain the elements Al, Fe, Co, Ni, and Mo. The elements Al, Fe, Co, and Mo are mainly attached to the surface of the alloy in the form of oxides, while Ni is mainly present in the form of hydroxides and oxides. According to research, the alloy Al 2p_{3/2} splits into two peaks with binding energies of 72.2 eV and 73.85 eV, which correspond to the metallic state Al (Al⁰) and the oxidized state Al₂O₃ (Al³⁺), respectively. Fe 2p_{3/2} shows two peaks at binding energies of 709.3 eV and 712 eV, representing the oxidation states of FeO (Fe²⁺) and Fe₂O₃ (Fe³⁺), respectively. The element Fe is relatively active, and the reaction in an aqueous solution may produce compounds such as FeO, Fe₂O₃, Fe₃O₄, and FeOOH. FeO is unstable and may continue to oxidize in the air. FeO is unstable and may continue to oxidize in air to Fe₂O₃ and Fe₃O₄ [24], which are mainly produced according to the XPS peak. In passive films, the element Co usually forms different compounds, which results in better film densities and adsorption. The three peaks of Co 2p_{3/2} at binding energies of 778.9, 780.7, and 782.3 eV represent Co(Co⁰), Co₃O₄, and Co(OH)₂, respectively, based on the peak intensities relative to the metallic state of Co, whose oxide can be judged based on the peak intensities to show that the element Co is mainly ionized into oxide and hydroxide forms on the metal surface. The two peaks of Ni 2p_{3/2} at binding energies of 854.9 and 855.9 eV represent NiO and Ni(OH)₂, respectively. Ni is more difficult to oxidize, hence the small amounts of NiO and Ni(OH)₂ observed in the passive films [25–27]. The three Mo 3d_{5/2} peaks at binding energies of 227.4, 231.8, and 232.3 eV correspond to Mo, MoO₂, and MoO₃, respectively. The elemental valence of Mo ranges from +2 to +6 and is generally attached to the passive film in the form of MoO₂ and MoO₃. According to the literature [28], in a neutral or alkaline solution environments, MoO₂ is further oxidized to MoO₄²⁻ ions attached to the surface of the passive film during its formation, which also protects the passive film to some extent from Cl⁻ attack. Thus, the element Mo contributes to enhancing the protective properties of the alloy passivation film. In addition to this, O can be found mainly in the form of hydroxide ions and oxygen ions, which are the main components in the generation of passive films on the surface of the alloy. The cation composition and species ratios of Al, Fe, Co, Ni, and Mo in the alloy passive film are shown in Figure 8b. Quantitative results show that the alloy surface passive film has large amounts of Al, Fe, and Co cations and lacks cations of Mo and Ni. In aqueous solutions, the process by which electrochemical corrosion of metals occurs is usually divided into the oxidative dissolution of the metal anode and reduction reactions of the anions. Metals lose electrons to form metal cations that react with anions to produce insoluble substances on the surface of the substrate, resulting in the active dissolution of the metal surface and a reduction in the contact area, hindering the attack of aggressive ions and preventing further dissolution of the metal. As Al is an active metal, it will complex with halogen atoms, and the Cl⁻ ions in solution will cause the destruction of the dense film structure of Al₂O₃ while the solubility of Al³⁺ in solution becomes greater, resulting in the corrosive dissolution of the alloy substrate [29,30]. The equation for this reaction is as follows:



To a certain extent, this explains the absence of stable passivation generation in the polarization curve of the AlFeCoNiMo_{0.2} high-entropy alloy in the environment of 3.5 wt% NaCl solution. The elements Fe, Co, and Ni form metal oxides on the surface of the alloy and play a positive role in the growth of the passive film. At the same time, Cl⁻ will compete with H₂O and OH⁻ in solution to adsorb elemental Ni on the metal surface and react with it to form (NiCl⁻)_{ad}, which further combines with water molecules to form (NiOHCl)⁻_{ad} complexes, resulting in the presence of elemental Ni in the form of oxides and hydroxides on the alloy surface.

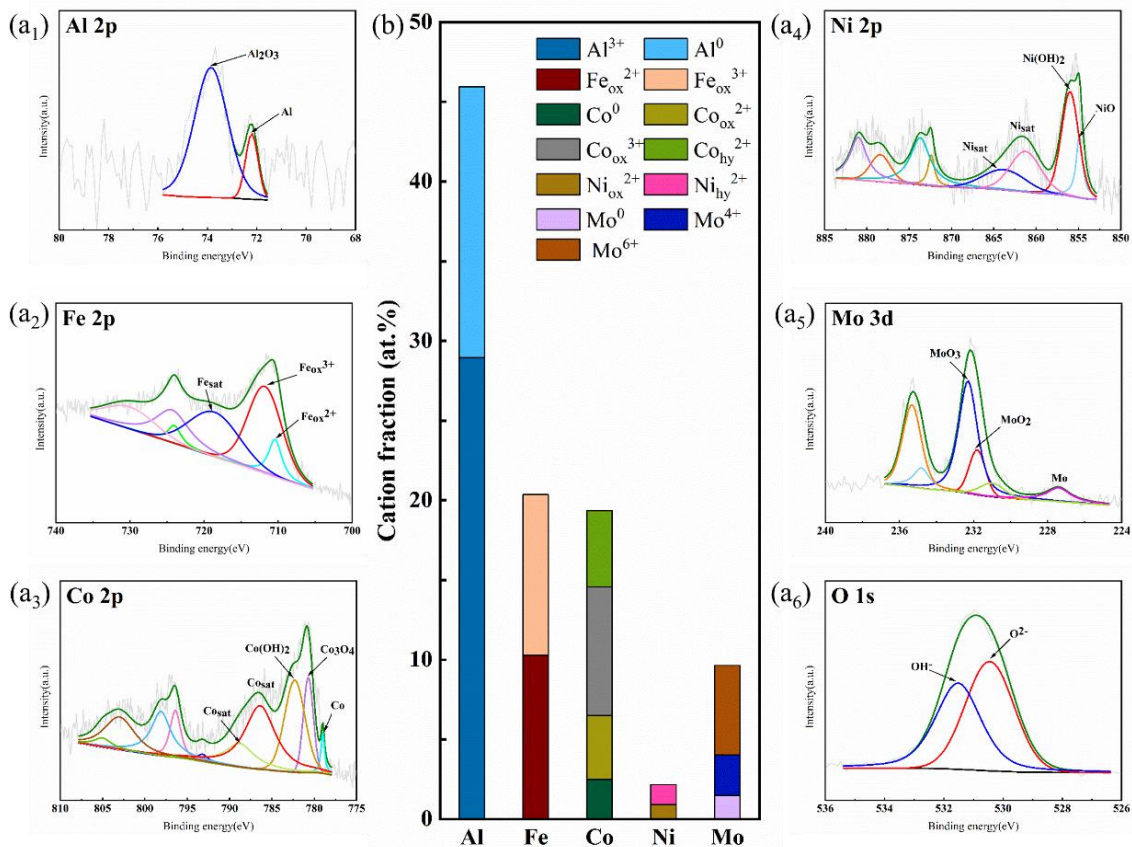


Figure 8. XPS spectra of as-cast AlFeCoNiMo_{0.2} HEA after polarization in 3.5 wt% NaCl solution: (a₁) Al 2p (a₂) Fe 2p (a₃) Co 2p (a₄) Ni 2p (a₅) Mo 3d (a₆) O 1s (b) element contents (at.%) in passive film.

Figure 9 displays the spectra of Al 2p, Fe 2p, Co 2p, Ni 2p, and Mo 3d in 0.5 M H₂SO₄ solution. The three O 1s peaks are H₂O, O₂, and OH⁻, respectively. A significant amount of OH⁻ accumulates in the topmost layer of the passive film and participates in the reaction that produces hydroxide. The bound water of the film surface, H₂O, can react with free metal cations to produce metal compounds, which can have some repairing effects on the film structure [31,32]. At binding energies of 73.7 eV and 75.9 eV, Al 2p_{3/2} separated into two peaks that correspond to the metallic state Al (Al⁰) and the oxidized state Al₂O₃ (Al³⁺), respectively. The two peaks of Fe 2p_{3/2} with binding energies of 710.4 eV and 711.8 eV correspond to Fe₂O₃ and FeOOH, wherein the hydroxyl group adsorbs to produce significant quantities of FeOOH, and the element Fe is readily and preferentially oxidized. The two peaks of Co 2p_{3/2} represent Co(OH)₂ and CoO, with binding energies of 780.9 and 782.9 eV, respectively. NiO and Ni(OH)₂ are represented by the two peaks of Ni 2p_{3/2} at binding energies of 855.4 and 856.3 eV, respectively, and MoO₃ is represented by the peak of Mo 3d_{5/2} at 232.3 eV. The third peak of the O 1s spectrum obtained from the passive film on the alloy indicates bound water in the passive film. The bound water can act as an effective species to trap free metal ions in solution and form a new film that resists further corrosion.

The cation composition and species ratios of Al, Fe, Co, Ni, and Mo in the alloy passive film in the sulfuric acid solution environment are shown in Figure 9b. Quantitative results show that Al and Mo are mainly present on the alloy surface as oxides, while Fe, Co, and Ni are present as oxides and hydroxides. During polarization, the elements Fe and Co are oxidized preferentially. As the polarization time increases, the Fe diffusion rate in the passive film is high, and the iron oxide dissolves more readily in the sulfuric acid solution, resulting in a reduction in the elemental Fe content of the passive film. Regarding the element Co, it has been confirmed in the literature that in the solution environment of dilute sulfuric acid [33], the element Co does not contribute to the passivation of the alloy. At the beginning of electrochemical corrosion, a passive film with protective properties is generated on the Ni surface. As the corrosion time increases, the H^+ concentration in the solution near the passive film on the Ni surface increases, resulting in Ni^{2+} continuously dissolving into the solution so that the dissolution rate of the passive film on the alloy substrate surface is faster than the film formation rate of the substrate, which will reduce the corrosion resistance of the alloy. According to previous studies [34], no passive film is generated on the surface of pure Mo after constant potential polarization, and the corresponding passivation current density is mainly derived from the activation reaction occurring at the cathode. The greater the iron oxide content, the less stable the passive film is, but the addition of Mo can inhibit to some extent the activation of Fe in the alloy to dissolve into iron oxide. At the same time, the presence of oxidation in the passive film in the form of MoO_3 can reduce the corrosion dissolution rate of the alloy and can improve the corrosion resistance of the film, a view that has been confirmed [35]. The O 1s spectrum obtained via fitting was for O^{2-} , OH^- , and adsorbed water, indicating that the passive film at this point was a highly mixed oxide film with multi-elemental hydroxides and oxides.

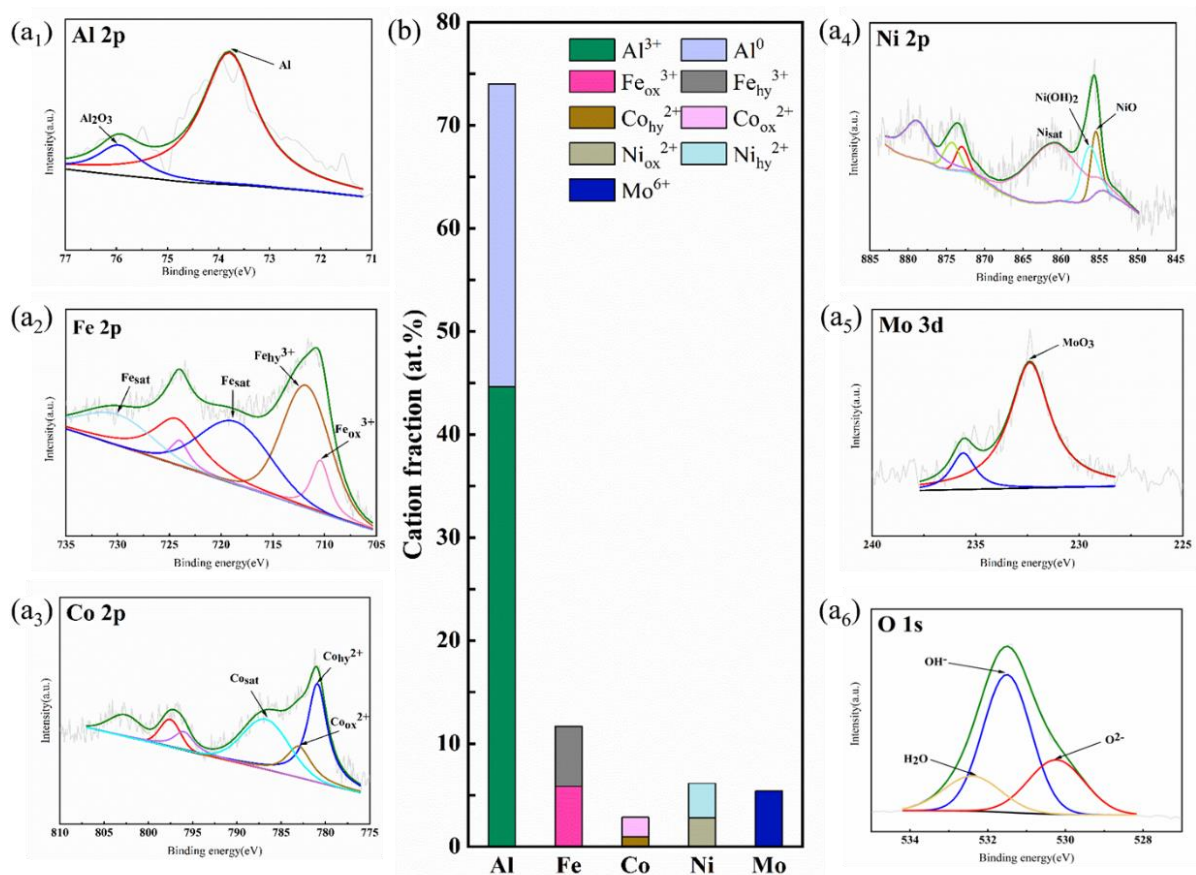


Figure 9. XPS spectra of as-cast AlFeCoNiMo_{0.2} HEA after polarization in 0.5 M H₂SO₄ solution: (a₁) Al 2p (a₂) Fe 2p (a₃) Co 2p (a₄) Ni 2p (a₅) Mo 3d (a₆) O 1s (b) element contents (at%) in passive film.

5. Conclusions

In this study, the AlFeCoNiMo_{0.2} high-entropy alloy was prepared and selected for different heat treatments at 800, 900, and 1000 °C. The microstructure was analyzed by XRD, SEM, and EDS under different conditions, and the corrosion resistances in 3.5 wt% NaCl and 0.5 mol/L H₂SO₄ solutions were investigated through dynamic potential polarization and impedance spectroscopy. The dissolution corrosion mechanism of passive films in different solutions was investigated through XPS tests. We explored the corrosion behavior of this alloy in different service environments, laying the theoretical and experimental groundwork for future use as an alternative material in the nuclear energy sector. From these considerations, we draw the following conclusions:

1. In the Cl[−] environment, the AlFeCoNiMo_{0.2} high-entropy alloy has a much lower corrosion current density in the as-cast state and significantly higher corrosion resistance than the annealed alloy. The reason for this is mainly due to the severe segregation of elements Al and Mo in the grain and grain boundaries after annealing, which enhances the occurrence of galvanic corrosion and leads to pitting corrosion in the grain;
2. In the SO₄^{2−} environment, the 900 °C annealed state AlFeCoNiMo_{0.2} high-entropy alloy has better corrosion resistance than other alloys. The electrochemical test results show that the alloys all undergo secondary passivation, producing two successive product films to protect the metal substrate. The corrosion morphology shows that the priority corrosion areas are mainly concentrated in the grain boundaries and nearby dendritic areas, mainly due to the enrichment of Mo elements at the grain boundaries of the alloy after annealing. However, Mo reduces the corrosion resistance of the alloy in sulphuric acid solution;
3. XPS results of cast AlFeCoNiMo_{0.2} after constant potential polarization in 3.5 wt% NaCl solution show that Al, Fe, Co, and Mo are mainly present on the alloy surface as oxides and Ni as oxides and hydroxides. The component Al in the alloy is an active metal and will form complexes with halogen atoms. The Cl[−] ions in the solution will destroy the dense film structure of Al₂O₃, making Al³⁺ more soluble in solution and causing corrosive dissolution of the passive film, resulting in no significant passivation of AlFeCoNiMo_{0.2} in the Cl[−] solution;
4. XPS results of cast AlFeCoNiMo_{0.2} after constant potential polarization in 0.5 mol/L H₂SO₄ solution show that Al and Mo are mainly present on the alloy surface as oxides; Fe, Co, and Ni are present on the alloy surface as oxides and hydroxides; and the passive film is an oxide film with a high mixture of multi-element hydroxides and oxides. The Mo element in the passive film inhibits the activation of Fe to dissolve into iron oxide and generate the protective component MoO₃ in the passive film, which inhibits the dissolution of the alloy and can improve the stability of the passive film.

Author Contributions: Conceptualization, Y.P. and G.Z.; methodology, Y.P.; software, Y.P.; validation, G.Z., Y.P. and J.H.; formal analysis, J.L.; investigation, H.Z.; resources, S.Z.; data curation, Y.P.; writing—original draft preparation, Y.P.; writing—review and editing, G.Z.; visualization, L.L.; supervision, L.C.; project administration, X.C.; funding acquisition, L.C. All authors have read and agreed to the published version of the manuscript.

Funding: This research was funded by [Natural Science Foundation] grant number [22-315-6-04] And The APC was funded by [zhouge@sut.edu.cn].

Institutional Review Board Statement: Not applicable.

Informed Consent Statement: Not applicable.

Data Availability Statement: No new data were created or analyzed in this study. Data sharing is not applicable to this article.

Conflicts of Interest: The authors declare no conflict of interest.

References

1. Yeh, J.W.; Chen, S.K.; Lin, S.J.; Gan, J.Y.; Chin, T.S.; Shun, T.T.; Tsau, C.H.; Chang, S.Y. Nanostructured high-entropy alloys with multiple principal elements: Novel alloy design concepts and outcomes. *Adv. Eng. Mater.* **2004**, *6*, 299–303. [[CrossRef](#)]
2. Cantor, B.; Chang, I.T.H.; Knight, P.; Vincent, A.J.B. Microstructural development in equiatomic multicomponent alloys. *Mat. Sci. Eng. A* **2004**, *375*, 213–218. [[CrossRef](#)]
3. Tsai, M.H.; Yeh, J.W. High-entropy alloys: A critical review. *Mater. Res. Lett.* **2014**, *2*, 107–123. [[CrossRef](#)]
4. Ye, Y.F.; Wang, Q.; Lu, J.; Liu, C.T.; Yang, Y. High-entropy alloy: Challenges and prospects. *Mater. Today* **2016**, *19*, 349–362. [[CrossRef](#)]
5. Xiao, Y.; Zou, Y.; Ma, H.; Sologubenko, A.S.; Maeder, X.; Spolenak, R.; Wheeler, J.M. Nanostructured NbMoTaW high entropy alloy thin films: High strength and enhanced fracture toughness. *Scr. Mater.* **2019**, *168*, 51–55. [[CrossRef](#)]
6. Li, D.; Zhang, Y. The ultrahigh charpy impact toughness of forged $\text{Al}_x\text{CoCrFeNi}$ high entropy alloys at room and cryogenic temperatures. *Intermetallics* **2016**, *70*, 24–28. [[CrossRef](#)]
7. Ma, S.G. Creep resistance and strain-rate sensitivity of a $\text{CoCrFeNiAl}_{0.3}$ high-entropy alloy by nanoindentation. *Mater. Res. Express* **2019**, *6*, 126508. [[CrossRef](#)]
8. Cao, T.; Chang, J.; Zhao, J.; Cheng, C.; Wang, R.; Wang, H. The influence of Al elements on the structure and the creep behavior of $\text{Al}_x\text{CoCrFeNi}$ high entropy alloys. *Mater. Lett.* **2016**, *164*, 344–347. [[CrossRef](#)]
9. Hsu, C.Y.; Yeh, J.W.; Chen, S.K.; Shun, T.T. Wear resistance and high-temperature compression strength of FCC $\text{CuCoNiCrAl}_{0.5}\text{Fe}$ alloy with boron addition. *Metall. Mater. Trans. A* **2004**, *35*, 1465–1469. [[CrossRef](#)]
10. Nene, S.S.; Frank, M.; Liu, K.; Sinha, S.; Mishra, R.S.; McWilliams, B.A.; Cho, K.C. Corrosion-resistant high entropy alloy with high strength and ductility. *Scr. Mater.* **2019**, *166*, 168–172. [[CrossRef](#)]
11. Chou, Y.L.; Yeh, J.W.; Shih, H.C. The effect of molybdenum on the corrosion behaviour of the high-entropy alloys $\text{Co}_{1.5}\text{CrFeNi}_{1.5}\text{Ti}_{0.5}\text{Mo}_x$ in aqueous environments. *Corros. Sci.* **2010**, *52*, 2571–2581. [[CrossRef](#)]
12. Chou, H.P.; Chang, Y.S.; Chen, S.K.; Yeh, J.W. Microstructure, thermophysical and electrical properties in $\text{Al}_x\text{CoCrFeNi}$ ($0 \leq x \leq 2$) high-entropy alloys. *Mat. Sci. Eng. B* **2009**, *163*, 184–189. [[CrossRef](#)]
13. Wang, W.R.; Wang, W.L.; Wang, S.C.; Tsai, Y.C.; Lai, C.H.; Yeh, J.W. Effects of Al addition on the microstructure and mechanical property of $\text{Al}_x\text{CoCrFeNi}$ high-entropy alloys. *Intermetallics* **2012**, *26*, 44–51. [[CrossRef](#)]
14. Kao, Y.F.; Chen, S.K.; Chen, T.J.; Chu, P.C.; Yeh, J.W.; Lin, S.J. Electrical, magnetic, and hall properties of $\text{Al}_x\text{CoCrFeNi}$ high-entropy alloys. *J. Alloys Compd.* **2011**, *509*, 1607–1614. [[CrossRef](#)]
15. Yang, H.O.; Shang, X.L.; Wang, L.L.; Wang, Z.J.; Wang, J.C.; Lin, X. Effect of constituent elements on the corrosion resistance of single-phase CoCrFeNi high-entropy alloys in NaCl solution. *Acta Metall. Sin.* **2018**, *54*, 905–910.
16. Niu, Z.Z.; Wang, Y.Z.; Geng, C.; Xu, J.; Wang, Y. Microstructural evolution, mechanical and corrosion behaviors of as-annealed CoCrFeNiMo_x ($x = 0, 0.2, 0.5, 0.8, 1$) high entropy alloys. *J. Alloys Compd.* **2020**, *820*, 153273. [[CrossRef](#)]
17. Wang, W.; Wang, J.; Sun, Z.H.; Li, J.T.; Li, L.F.; Song, X.; Wen, X.D.; Xie, L.; Yang, X. Effect of Mo and aging temperature on corrosion behavior of $(\text{CoCrFeNi})_{100-x}\text{Mo}_x$ high-entropy alloys. *J. Alloys Compd.* **2020**, *812*, 152139. [[CrossRef](#)]
18. Lin, C.M.; Tsai, H.L.; Bor, H.Y. Effect of aging treatment on microstructure and properties of high-entropy $\text{Cu}_{0.5}\text{CoCrFeNi}$ alloy. *Intermetallics* **2010**, *18*, 1244–1250. [[CrossRef](#)]
19. Wen, X.; Jin, G.; Pang, X.J.; Cai, Z.B.; Zhang, Z.H.; Cui, X.F.; Wang, H.D.; Xu, B.S. Effect of heat treatment on microstructure and corrosion resistance of NiCrCoTiV high-entropy alloy prepared by vacuum hot-pressing sintering. *Mater. Rep. B* **2017**, *31*, 79–83.
20. Zhang, X.; Guo, J.; Zhang, X.; Song, Y.; Li, Z.; Xing, X.; Kong, D. Influence of remelting and annealing treatment on corrosion resistance of AlFeNiCoCuCr high entropy alloy in 3.5wt% NaCl solution. *J. Alloys Compd.* **2018**, *775*, 565–570. [[CrossRef](#)]
21. Fernandes, D.M.; Montes, R.H.O.; Almeida, E.S.; Nascimento, A.N.; Oliveira, P.V.; Richter, E.M.; Munoz, R.A.A. Storage stability and corrosive character of stabilised biodiesel exposed to carbon and galvanised steels. *Fuel* **2013**, *107*, 609–614. [[CrossRef](#)]
22. Sugimoto, K.; Sawada, Y. The role of molybdenum additions to austenitic stainless steels in the inhibition of pitting in acid chloride solutions. *Corros. Sci.* **1997**, *17*, 425–445. [[CrossRef](#)]
23. Lu, P.; Saal, J.E.; Olson, G.B.; Li, T.S.; Sahu, S.; Swanso, O.J.; Frankel, G.S.; Gerard, A.; Scully, J.R. Computational design and initial corrosion assessment of a series of non-equimolar high entropy alloys. *Scr. Mater.* **2019**, *172*, 12–16. [[CrossRef](#)]
24. Ming, J.; Wu, M.; Shi, J.J. Passive film modification by concrete carbonation: Re-visiting a corrosion-resistant steel with Cr and Mo. *Cement. Concr. Comp.* **2021**, *123*, 104178. [[CrossRef](#)]
25. Olsson, C.O.A.; Landolt, D. Passive films on stainless steels—Chemistry, structure and growth. *Electrochim. Acta* **2003**, *48*, 1093–1104. [[CrossRef](#)]
26. Jiang, R.J.; Wang, Y.W.; Wen, X.; Chen, C.F.; Zhao, J.M. Effect of time on the characteristics of passive film formed on stainless steel. *Appl. Surf. Sci.* **2017**, *412*, 214–222. [[CrossRef](#)]
27. Abdallah, M.; Salem, M.M.; Zaafarany, I.A. Corrosion performance of stainless steel and nickel alloys in aqueous sodium hydroxide as revealed from cyclic voltammetry and potentiodynamic anodic polarization. *Orient. J. Chem.* **2017**, *33*, 2875–2883. [[CrossRef](#)]
28. Pourbaix, M. Atlas of electrochemical equilibria in aqueous solutions. *Electroanal. Chem.* **1967**, *13*, 471.
29. Aliyu, A.; Srivastava, C. Corrosion behavior and protective film constitution of AlNiCoFeCu and AlCrNiCoFeCu high entropy alloy coatings. *Surf. Interfaces* **2021**, *27*, 101481. [[CrossRef](#)]

30. Nascimento, C.B.; Donatus, U.; Ríos, C.T.; Antunes, R.A. Passive film composition and stability of CoCrFeNi and CoCrFeNiAl high entropy alloys in chloride solution. *Mater. Chem. Phys.* **2021**, *267*, 124582. [[CrossRef](#)]
31. Luo, H.; Zou, S.W.; Chen, Y.H.; Li, Z.M.; Du, C.W.; Li, X.G. Influence of carbon on the corrosion behaviour of interstitial equiatomic CoCrFeMnNi high-entropy alloys in a chlorinated concrete solution. *Corros. Sci.* **2020**, *163*, 108287. [[CrossRef](#)]
32. Okamoto, G. Passive film of 18-8 stainless steel structure and its function. *Corros. Sci.* **1973**, *13*, 471–489. [[CrossRef](#)]
33. Dai, C.D.; Zhao, T.L.; Du, C.W.; Liu, Z.Y.; Zhang, D.W. Effect of molybdenum content on the microstructure and corrosion behavior of FeCoCrNiMo_x high-entropy alloys. *J. Mater. Sci. Technol.* **2020**, *46*, 64–73. [[CrossRef](#)]
34. Falkenberg, F.; Raja, V.S.; Ahlberg, E. An alternative explanation for the apparent passivation of molybdenum in 1 mol/L hydrochloric acid. *J. Electrochem. Soc.* **2001**, *148*, B132. [[CrossRef](#)]
35. Hashimoto, K.; Asami, K.; Kawashima, A.; Habazaki, H.; Akiyama, E. The role of corrosion-resistant alloying elements in passivity. *Corros. Sci.* **2007**, *49*, 42–52. [[CrossRef](#)]

Disclaimer/Publisher’s Note: The statements, opinions and data contained in all publications are solely those of the individual author(s) and contributor(s) and not of MDPI and/or the editor(s). MDPI and/or the editor(s) disclaim responsibility for any injury to people or property resulting from any ideas, methods, instructions or products referred to in the content.